DMT induces a transient destabilization of whole-brain dynamics

Juan Ignacio Piccinini[1*], Yonatan Sanz Perl[1,2], Carla Pallavicini[1], Gustavo Deco[2,3,4,5,] Morten Kringelbach[6,7,8], David Nutt[9], Robin Carhart-Harris[10], Christopher Timmermann[9], Enzo Tagliazucchi[1,11*]

[1]Universidad de Buenos Aires, Facultad de Ciencias Exactas y Naturales, Departamento de Física, and CONICET - Universidad de Buenos Aires, Instituto de Física Aplicada e Interdisciplinaria (INFINA). Buenos Aires, Argentina.

[2]Center for Brain and Cognition, Computational Neuroscience Group, Department of Information and Communication Technologies, Universitat Pompeu Fabra, Barcelona, Spain

[3]Institució Catalana de la Recerca i Estudis Avançats (ICREA), Barcelona, Spain

[4]Department of Neuropsychology, Max Planck Institute for Human Cognitive and Brain Sciences, Leipzig, Germany

[5]School of Psychological Sciences, Monash University, Melbourne, Clayton VIC, Australia

[6]Centre for Eudaimonia and Human Flourishing, University of Oxford, Oxford, UK

[7]Department of Psychiatry, University of Oxford, Oxford, UK

[8]Center for Music in the Brain, Department of Clinical Medicine, Aarhus University, Denmark

[9]Centre for Psychedelic Research, Division of Psychiatry, Department of Brain Sciences, Imperial College London, London, UK

[10]Psychedelics Division, Neuroscape, Department of Neurology, University of California San Francisco, San Francisco, California, USA

[11]Latin American Brain Health Institute (BrainLat), Universidad Adolfo Ibañez, Santiago, Chile

* Corresponding authors: Juan Piccinini (piccijuan@gmail.com), Enzo Tagliazucchi (tagliazucchi.enzo@googlemail.com)

Abstract

The transition towards the brain state induced by psychedelic drugs is frequently neglected in favor of a static description of their acute effects. We used a time-dependent whole-brain model to reproduce large-scale brain dynamics measured with fMRI from 15 volunteers under 20 mg of bolus intravenous N,N-Dimethyltryptamine (DMT), a short-lasting psychedelic. To capture the transient effects of DMT, we parametrized the proximity to a global bifurcation using a pharmacokinetic equation and adopted the empirical functional connectivity dynamics (FCD) as optimization target. Post-administration, DMT rapidly destabilized brain dynamics, peaking after ≈5 minutes, followed by a recovery to baseline. Simulated perturbations revealed a transient of heightened reactivity, where stimulation maximally impacted the FCD. Local reactivity concentrated in fronto-parietal regions and visual cortices, and correlated with serotonin 5HT2a receptor density, the primary target of psychedelics. These advances suggest a mechanism to explain key features of the psychedelic state, such as increased brain complexity, diversity, and flexibility. Our model also predicts that the temporal evolution of these features aligns with pharmacokinetics. These results contribute to understanding how psychedelics introduce a transient where minimal perturbations can achieve a maximal effect, shedding light on how short psychedelic episodes may extend an overarching influence over time.

Introduction

Psychedelic drugs offer an opportunity to investigate how changes in the brain across multiple spatiotemporal scales interact with human consciousness and cognition (Kwan, Olson, Preller, & Roth, 2022). At the molecular level, psychedelics bind to the serotonin 5HT2a receptor (Nichols, 2016), recruiting specific intracellular signaling pathways that are different from those implicated in the action of non-psychedelic 5HT2A agonists (Gonzalez-Maeso et al., 2007; Wallach et al., 2023). The subjective effects of psychedelics may also depend on other pharmacological and non-pharmacological factors (Zamberlan et al., 2018), the latter including the context of drug intake and the mindset of the user (Carhart-Harris et al., 2018). At the systems level, psychedelics increase global network integration measured with functional magnetic resonance imaging (fMRI) (Bedford et al., 2023; Carhart-Harris et al., 2016; Luppi et al., 2021; Preller et al., 2018; Tagliazucchi et al., 2016; Timmermann et al., 2023), and evidence from multiple modalities links their effects to increased entropy and complexity of spontaneous brain activity fluctuations (Herzog et al., 2023; Lebedev et al., 2016; Pallavicini et al., 2021; Schartner, Carhart-Harris, Barrett, Seth, & Muthukumaraswamy, 2017; Tagliazucchi, Carhart-Harris, Leech, Nutt, & Chialvo, 2014; Timmermann et al., 2019; Viol, Palhano-Fontes, Onias, de Araujo, & Viswanathan, 2017). An integrative understanding of psychedelic action would require the identification of causal mechanisms behind these empirical observations, from molecules to subjective experience (Kwan et al., 2022).

In recent years, generative whole-brain activity models have been increasingly adopted to test potential mechanisms underlying neuroimaging data, including successful applications to the specific case of psychedelic compounds psilocybin and lysergic acid diethylamide (LSD) (Cofre et al., 2020). In these two case studies, biophysical models consisting of local excitatory and inhibitory populations with excitatory long-range connections were used to provide evidence supporting psychedelic-induced modulation of 5HT2a synaptic scaling (Burt et al., 2021; Deco et al., 2018; Kringelbach et al., 2020). Herzog and colleagues implemented a similar model to show that 5HT2a receptor

stimulation is consistent with increased brain-wide entropy (Herzog et al., 2023), in agreement with the theoretical model of psychedelic action proposed by Carhart-Harris (Carhart-Harris et al., 2014). As an alternative, the use of simpler models fitted to the empirical measurements can help shift the focus from the neurobiological details of drug action to the qualitative aspects of brain dynamics that characterize the acute effects of psychedelics (Girn et al., 2023). This approach was followed to demonstrate that LSD increases the complexity of spontaneous brain activity (Jobst et al., 2021), an observation consistent with previous studies showing an expanded repertoire of brain states with facilitated transitions between them (Singleton et al., 2022; Tagliazucchi et al., 2014), constituting a potential mechanism for the psychedelic-induced enhancement of neural and cognitive flexibility (Doss et al., 2021). Moreover, the dynamical characterization of psychedelic action reveals a scenario opposite to that of unconsciousness, reflecting a reduction in the repertoire of brain states and an increase in their stability against perturbations (Demertzi et al., 2019; Girn et al., 2023; Solovey et al., 2015).

To date, whole-brain models have been used to investigate the mechanisms underlying the steady state effects of LSD and psilocybin, two relatively long-lasting psychedelic drugs with effects extending over several hours. Therefore, it is currently unknown whether the putative mechanisms of psychedelic action identified by these models also extend to the transitions between the baseline and the acute effects. Time-dependent models capable of fitting dynamics across transitions are necessary to distinguish between the neurochemical modulation of brain activity, aligned with the drug pharmacokinetics, and the indirect effects of factors linked to the interplay between expectations, subjective effects and the short-term impact of the experience on the emotional state of the subjects, among others (Kwan et al., 2022). Moreover, developing computational models sensitive to slow temporal fluctuations in brain activity may contribute to determine whether the pharmacology of certain psychedelics is multi-phasic, as has been proposed for the case of LSD (Marona-Lewicka, Thisted, & Nichols, 2005). The short-lasting psychedelic effects of DMT are ideally suited for this

purpose, as they are highly dynamic and give way to the recovery of the baseline state after around 30 minutes (Strassman, 1996). Making progress in this direction, a recent study established that specific EEG features of the DMT state are correlated with the serum concentration of the drug (Eckernas, Timmermann, Carhart-Harris, Roshammar, & Ashton, 2023). However, the dynamical principles behind the transition to altered consciousness remain to be addressed by modeling efforts.

In this work, we adopted a model previously used to investigate the effects of psychedelic drugs (Jobst et al., 2021), introducing time dependency in the parameter governing the proximity to dynamical criticality, i.e. the transition between qualitatively different dynamics (noise vs. oscillations as shown in Piccinini et al. 2021). To model the relatively short-lasting effects induced by DMT, the temporal evolution of the model bifurcation parameter was constrained to represent a simplified version of DMT pharmacokinetics (Salway & Wakefield, 2008). The optimization of the free parameters underlying this temporal evolution allowed us to reproduce the empirical functional connectivity dynamics (FCD) (Deco, Kringelbach, Jirsa, & Ritter, 2017), and subsequently the optimal peak intensity and latency for DMT vs. a placebo control condition. Finally, we investigated the stability of the simulated dynamics against external perturbations, thus assessing potential correlations between the local regional reactivity and the density of 5HT2a receptors, the main pharmacological target of DMT (Nichols, 2016).

Results

Figure 1 provides an outline of the methods and the overall procedure. Following previous work, the local dynamics in the whole-brain model were given by Stuart-Landau nonlinear oscillators, with a bifurcation at $a=0$ (Deco et al., 2017). For $a>0$ the model presents stable oscillations, while $a<0$ results in stable spirals which extinguish the oscillation amplitude until the dynamics are dominated by the additive noise term, $\eta(t)$. Close to the bifurcation (i.e. dynamic criticality), the noise introduces

spontaneous switches between both regimes, resulting in oscillations with complex amplitude fluctuations. To model the time-dependent changes introduced by DMT, we put forward an assumed equation for the bifurcation parameter $a(t)$ given by the gamma function shown in Fig. 1. Parameters λ and β determine the peak amplitude and its latency, respectively. For an adequate choice of parameters, this function rises rapidly and then presents a slow decay, constituting an approximate description of the pharmacokinetics of bolus intravenous DMT administration (Salway & Wakefield, 2008). The local Stuart-Landau nonlinear oscillators were coupled using an averaged structural connectivity matrix inferred using diffusion tensor imaging (DTI) from healthy individuals and scaled by the global coupling parameter G. Since we aimed to reproduce the temporal evolution introduced by the short-acting effects of DMT, we optimized the gamma function parameters λ and β to fit the reproduction of the mean FCD computed from 15 participants, which contains in its i, j entry the similarity between functional connectivity (FC) matrices computed over short windows starting at time points i and j (see Methods). Note that in contrast to previous applications of this model to resting state data (Deco et al., 2018; Deco et al., 2017; E. C. Hansen, Battaglia, Spiegler, Deco, & Jirsa, 2015; Piccinini et al., 2021), we did not optimize the statistical similarity between the empirical and simulated FCD matrices; instead, we employed the Frobenius distance for their comparison, as we were interested in capturing the temporal evolution introduced by DMT.

To determine the optimal gamma function parameters to reproduce the whole-brain dynamics represented by the FCD, we performed an exhaustive exploration of all pairwise combinations of λ and β within a range of values compatible with the expected DMT pharmacokinetics (see Methods). The results of this exploration are shown in Fig. 2A for the placebo (left) and DMT conditions (right), with lower values indicating a better model fit. For the placebo condition, the optimal values were located within a large region of comparatively low amplitude and variable latency, evidencing a weak temporal dependency without a clearly defined peak of maximal intensity. Conversely, for DMT this region was displaced and reduced to encompass shorter and less variable latencies, together with

larger amplitude values. Figure 2B represents the empirical (left column) and optimal simulated (right column) FCD matrices for the placebo (first row) and DMT conditions (second row). Note that the two diagonal blocks of the FCD matrices separate the baseline (see Fig.1, "Functional connectivity dynamics") and post-administration periods. It can be seen that the model is capable of approximating this temporal structure, as well as the overall intensity of the matrix element values.

After determining the optimal λ and β for each independent run of the simulation, we explored the corresponding $a(t)$ plots displayed in Fig. 3A for placebo and DMT, with thicker lines indicating the mean across all simulations. This figure shows that dynamics start from a baseline of sustained oscillations at $a=0.07$. After DMT infusion, we observed a sharp and rapid decrease of $a(t)$ which displaced whole-brain dynamics towards the bifurcation at $a=0$. After peaking after ≈ 5 minutes, the parameter $a(t)$ gradually recovered towards baseline values at the end of the scanning session. In contrast, results for the placebo condition showed a lower peak amplitude combined with longer latencies, to the point where the peaks were not reached during the scanning session. As a consequence, $a(t)$ for the placebo condition approximated the constant baseline value with comparatively smaller temporal variation. Figure 3B summarizes the differences between the dynamics of $a(t)$ found for placebo and DMT in the two-dimensional space spanned by λ and β, where each point represents optimal values for an independent run of the simulation, and the larger full circles indicate the mean across all simulations. For the DMT condition, we could observe that λ and β were clustered in the upper left corner, indicating comparatively low latencies and high amplitude peaks ($\lambda=159.3 \pm 7$, $\beta=284 \pm 37$, 95% confidence interval [CI]). Conversely, the placebo condition resulted in low amplitude values and more variable latencies, skewed towards larger values relative to DMT ($\lambda=65.6 \pm 9$, $\beta=588 \pm 69$, 95% CI). Both clusters of values could be clearly separated, supporting the finding of qualitatively different $a(t)$ dynamics between conditions.

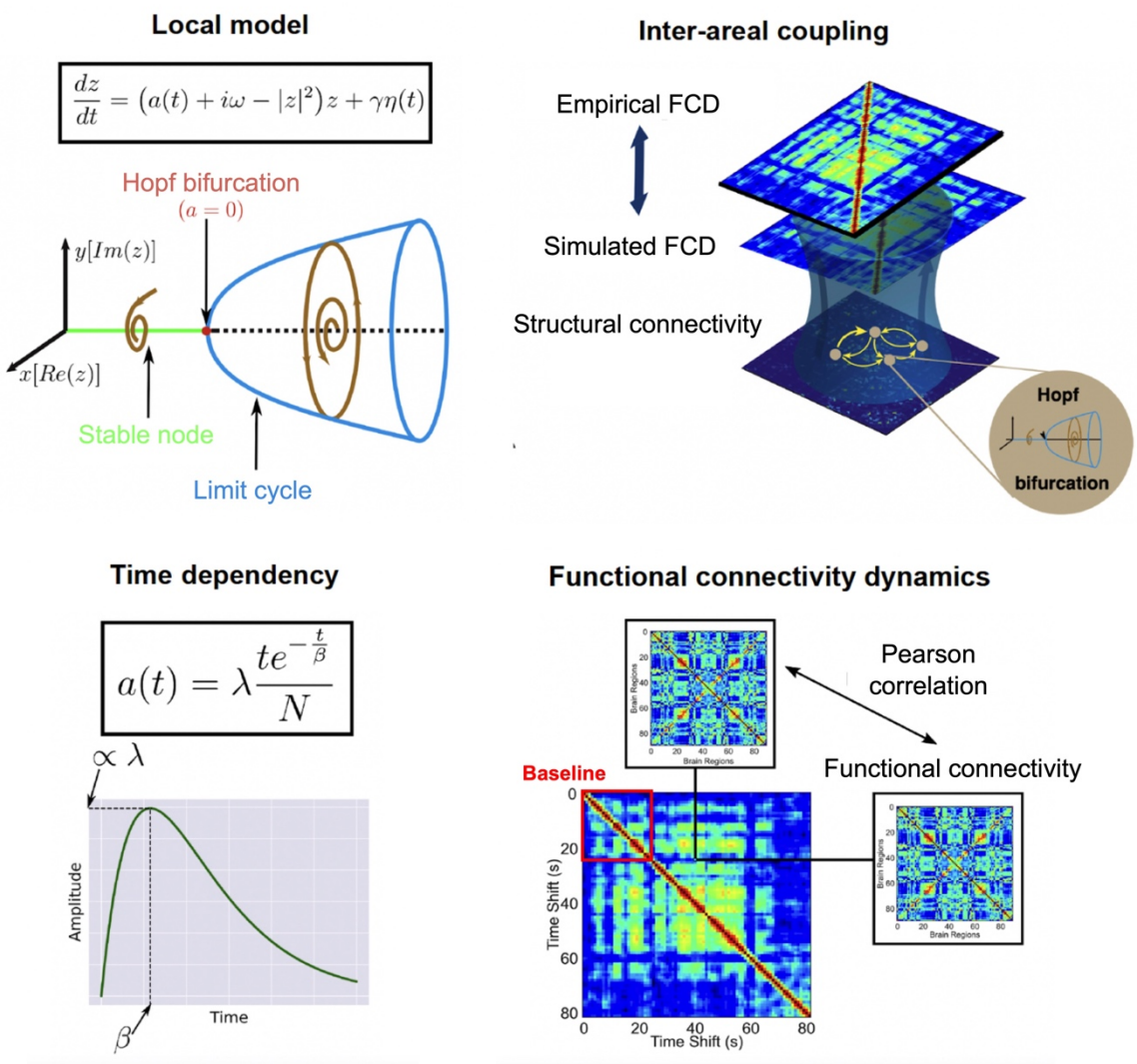

Figure 1. Overview of the whole-brain model and the choice of optimization target. The upper left panel ("Local model") presents the dynamics of a single node, consisting of a Stuart-Landau nonlinear oscillator with bifurcation parameter a, and the imaginary and real part of complex variable z vs. a, showing a transition between stable spirals and limit cycles at a=0. The bottom left panel ("Time dependency") presents the temporal parametrization of the bifurcation parameter a(t), given by a gamma function with parameters λ (peak amplitude) and β (peak latency). The upper right panel ("Inter-areal coupling") illustrates how the nodes were coupled following the structural connectivity given by DTI scaled by G to reproduce the empirical FCD. Finally, the bottom right panel ("Functional connectivity dynamics") shows the computation of the FCD matrix, which contains in its i, j entry the similarity between FC matrices computed over short windows starting at time points i and j. The diagonal block encased in red indicates the baseline period before the administration of DMT.

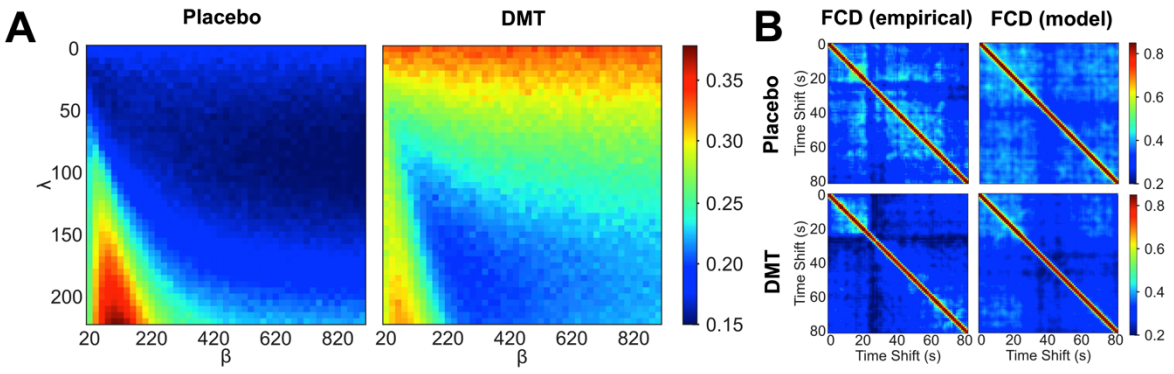

Figure 2. Exploration of the parameter space reveals different peak amplitude (λ) and latency (β) values for placebo vs. DMT (panel A). Panel B shows the empirical and optimal simulated FCD (columns) for the placebo and DMT conditions (rows).

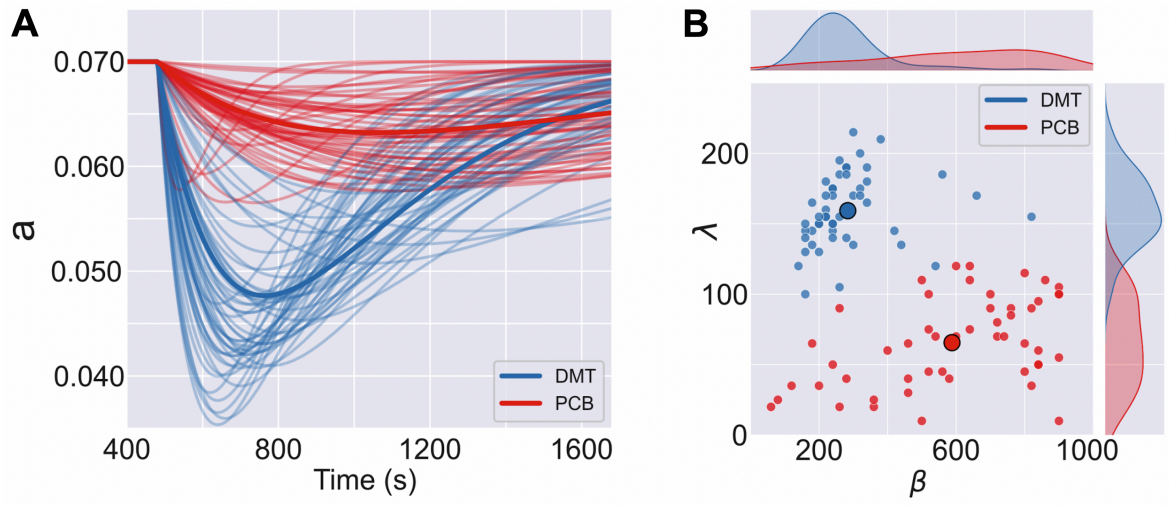

Figure 3. The temporal evolution of a(t) distinguishes between DMT and the placebo condition. A) a(t) for multiple independent runs of parameter optimization, compared between both conditions. Plots with thicker lines indicate the mean curves computed across simulation runs. B) Two-dimensional representation of the optimal model parameters, λ and β, both for placebo and DMT. Individual points indicate the outcome of independent runs of parameter optimization, while the larger full circles represent the average across simulation runs.

After determining the optimal parameters to fit the FCD, we used the resulting models to investigate the time-dependent effects of delivering external perturbations. This analysis was motivated in previous reports indicating that psychedelics increase the reactivity to external stimuli and facilitate transitions between brain metastable states (Jobst et al., 2021; Singleton et al., 2022). Based on these results, we hypothesized that DMT would result in a transient episode of more reactive brain dynamics, arising due to a destabilization of whole-brain dynamics, i.e. due to the increased proximity to dynamic criticality.

For this purpose, we introduced a periodic external perturbation at the frequency of the endogenous oscillations, which was previously shown to maximize the effect on the ongoing brain activity (Ipina et al., 2020; Jobst et al., 2017). We determined the reactivity to the perturbation at each time point, noted here by $\chi(t)$, by computing the derivative of the induced FCD changes with a numerical differentiation algorithm (see methods for more details). To facilitate the interpretation of the results, we introduced this perturbation at nodes located within six resting state networks (RSN) (Beckmann, DeLuca, Devlin, & Smith, 2005) known to encompass different functional brain systems: primary visual (Vis), extrastriate (ES), auditory (Aud), sensorimotor (SM), default mode (DM) and executive control (EC) cortices. Figure 4A shows $\chi(t)$ for each RSN, both for the placebo (top) and DMT (bottom) conditions. For the latter, it is clear that $\chi(t)$ is aligned with the expected evolution of drug effect intensity, with the largest reactivity obtained at the extrastriate visual cortex. In contrast, the time dependency of $\chi(t)$ was considerably less marked for the placebo group. Figure 4B displays the peak of $\chi(t)$, i.e. χ_{max}, for each RSN and for three different external perturbation intensities (F_{ext}), comparing the DMT and placebo conditions. Consistent with the results shown in Fig. 4A, the peak values were systematically lower in placebo vs. DMT for all intensities, indicating higher reactivity to external perturbations during the acute effects of the drug.

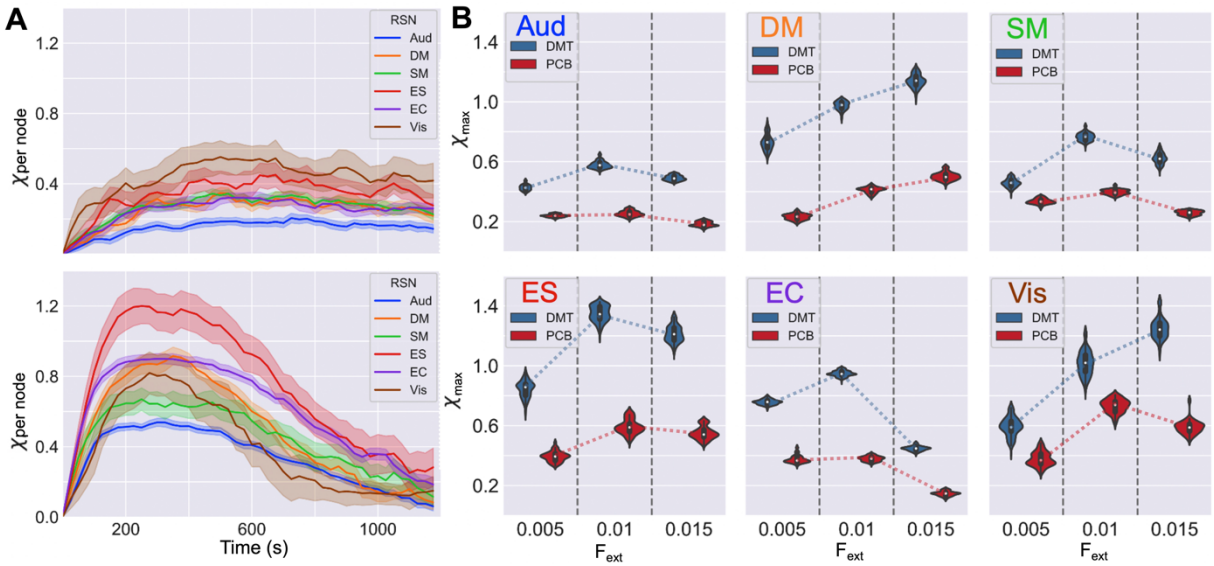

Figure 4. Time-dependent effect of simulated perturbations indicate higher reactivity for DMT vs. placebo. A) Reactivity $\chi(t)$ normalized by the number of nodes in the corresponding RSN, for placebo (top) and DMT (bottom). B) Plots of the peak $\chi(t)$ across time (χ_{max}) for each RSN and three different external perturbation intensities (F_{ext}).

Finally, we investigated the correlation between the 5HT2a receptor density (see Methods) and the peak reactivity (χ_{max}) across RSN. Based on the known pharmacological action of DMT (Nichols, 2016), we expected a positive correlation between these two variables, i.e. that RSN with higher 5HT2a receptor density would show higher χ_{max} values, and vice-versa. Figure 5A illustrates the spatial configuration of the RSN, while the mean 5HT2a receptor density per RSN is shown in Fig. 5B. To assess if the difference in χ_{max} between conditions can be attributed to the local density of serotonin receptors, we first computed the difference between the reactivity curves of DMT and placebo, resulting in $\Delta\chi(t)$. Figure 5C shows the peak of $\Delta\chi(t)$, $\Delta\chi_{max}$, vs. the 5HT2a receptor density of each RSN, together with the best least-squares linear fit. To estimate the significance of this correlation, we conducted a bootstrap procedure which resulted in the distribution of correlation coefficients (ρ) presented in the inset of this panel, with a mean value of $\rho \approx 0.9$. Figure 5D displays

the mean ρ ($\Delta\chi_{max}$ vs. 5HT2a receptor density) across a range of external perturbation intensities (F_{ext}). This plot indicates that low stimulation amplitudes exert an effect that is comparatively independent of the local 5HT2a receptor density. However, as the perturbation intensity increases, the receptor density becomes more relevant, peaking at ρ >0.9. Finally, as the intensity keeps increasing, the reactivity decouples again from the receptor density.

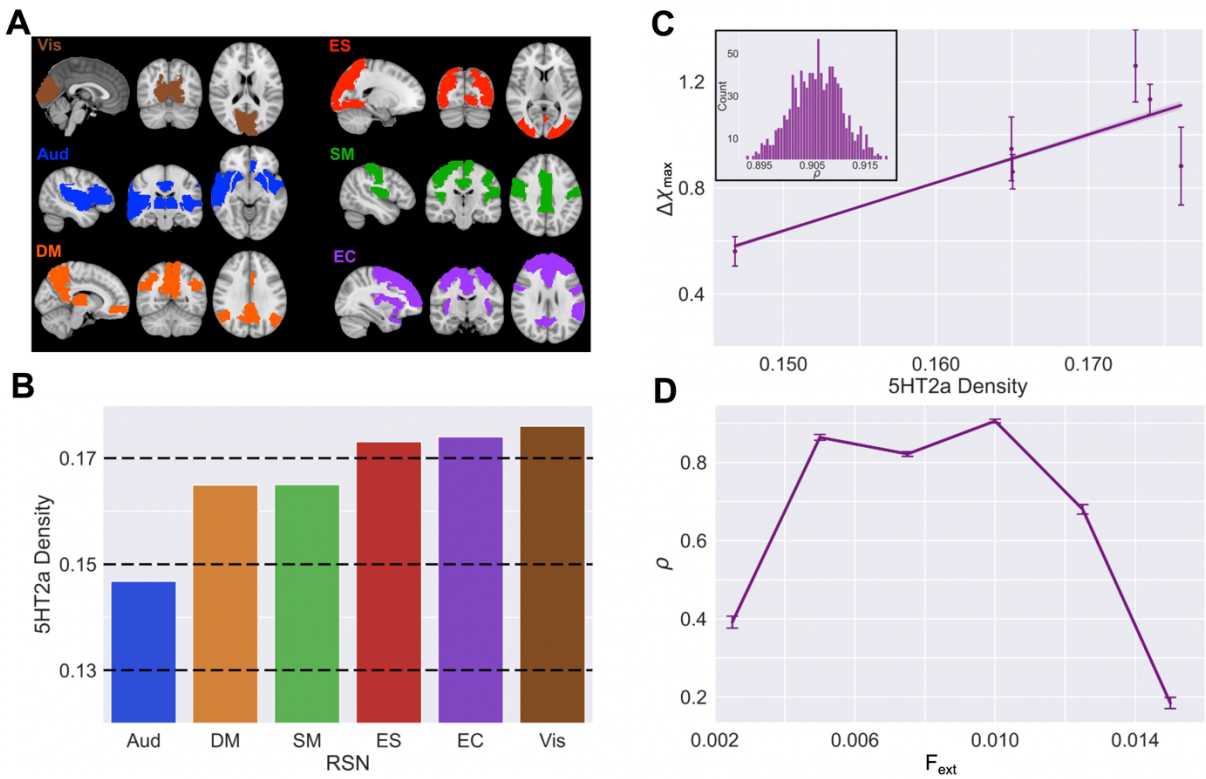

Figure 5. The peak differential reactivity to external perturbations ($\Delta\chi_{max}$) between DMT and placebo correlates with the local 5HT2a receptor density. A) Spatial configuration of the six RSN that constrained the simulated delivery of the perturbation (Vis: primary visual, ES: extrastriate, Aud: auditory, SM: sensorimotor, DM: default mode, EC: executive control), adapted from (Beckmann et al., 2005). B) Mean 5HT2a receptor density per RSN. C) Peak of $\Delta\chi(t)$, $\Delta\chi_{max}$, vs. the 5HT2a receptor density of each RSN (mean ± SEM) together with the best least-squares linear fit. The inset shows the distribution of correlation coefficients (ρ) obtained using a bootstrap procedure. D) Correlation coefficient ρ vs. the external perturbation intensity, F_{ext}.

Discussion

This study represents a first step towards the computational modeling of time-dependent psychedelic effects. Our main finding is that DMT destabilizes (i.e. brings closer to the global bifurcation point, or dynamic criticality) whole-brain dynamics, and that the extent of this destabilization is compatible with the characteristic pharmacokinetics of the drug, here constrained by a gamma function (Salway & Wakefield, 2008) Conversely, an inactive placebo resulted in extreme parameter values that flattened this function, thus approximating a constant value over time. A consequence of this loss of stability is the heightened sensitivity to external perturbations (Jobst et al., 2017), paralleling the dynamics of the bifurcation parameter and thus being maximal when the perturbation is applied in nodes belonging to RSN with high 5HT2a receptor density. This increased sensitivity may affect how the brain responds to incoming sensory stimuli under the effects of the drug, and may also impact on its capacity to amplify endogenous events linked to ongoing mentation and cognitive processing. Indeed, recent work showed that external stimulation delivered during the psychedelic state has stronger effects relative to a control condition, which include changes in the intensity of the experience as well as a substantial modification of entropy-based metrics of neural activity (Pedro A.M. Mediano, 2024)

Previous studies have used similar models to investigate the mechanisms underlying psychedelic-induced changes in fMRI resting state activity (Burt et al., 2021; Deco et al., 2018; Jobst et al., 2021; Kringelbach et al., 2020). However, these studies were concerned primarily with the steady state effects of the drugs, thus neglecting the analysis of periods when their intensity changes over time, such as the transitions between the baseline and the acute state. These transitions are difficult to capture for the oral administration of LSD or psilocybin, which results in a slower onset and a less marked transition towards the psychedelic state (Dolder et al., 2017; Holze, Becker, Kolaczynska, Duthaler, & Liechti, 2023). In contrast, the intravenous administration of DMT results in a brief psychedelic episode, with a sharp onset and a peak of subjective effects occurring a few minutes after

the infusion (Strassman, 1996). Our study shows that the whole-brain dynamics induced by DMT on fMRI data recapitulate this temporal evolution, which was not observed for the placebo. It is important to note that even if the intensity of the DMT effects is not reflected on the amplitude of the time-domain fMRI signals, whole-brain FC contains sufficient information to determine the temporal evolution of the DMT experience as shown by the optimal fit of the model to the FCD data.

The transient destabilization induced by DMT is consistent with multiple experimental results and theoretical accounts of psychedelic action in the human brain (Carhart-Harris et al., 2014). Drawing from the theory of bifurcations in dynamical systems, as the model approximates the bifurcation both the complexity and entropy of simulated brain activity are expected to increase (Herzog et al., 2023; Lebedev et al., 2016; Pallavicini et al., 2021; Schartner et al., 2017; Tagliazucchi et al., 2014; Timmermann et al., 2019; Viol et al., 2017), together an expansion in the repertoire of possible metastable states (Tagliazucchi, Carhart-Harris et al. 2014). Also near the bifurcation, the sensitivity of the system to external perturbations is maximized (Jobst et al., 2021; Jobst et al., 2017), predicting a larger response to an externally induced stimulation during the psychedelic state. Using non-invasive transcranial magnetic stimulation (TMS) combined with electroencephalography (EEG), Ort and colleagues could not find changes in cortical reactivity induced by psilocybin; however, they informed changes in spectral content and subjective experience linked to the stimulation (Ort et al., 2023). This result is partially consistent with our prediction, especially when taking into account the differences between TMS and a periodic perturbation delivered at the natural frequency of the endogenous oscillations. Empirically, this perturbation could be achieved by non-invasive methods such as transcranial alternating current stimulation (tACS) (Helfrich et al., 2014); however, to date this form of stimulation has not been investigated in participants undergoing the effects of psychedelic drugs.

Our results draw a parallel between the effects of DMT on whole-brain dynamics and the theory of dynamical and statistical criticality. The main difference between conditions was the behavior of the bifurcation parameter across time, resulting in values closer to the critical value coincident with the peak effects of DMT. This finding can be interpreted through the critical brain hypothesis, stating that the major features of brain dynamics can be explained by proximity to a second order phase transition (Chialvo, 2010; Cocchi, Gollo, Zalesky, & Breakspear, 2017). Near this critical point, the system exhibits divergent susceptibility (i.e. reactivity), allowing minor perturbations to propagate throughout the entire system (Tian, 2022). Extending this analogy, we can postulate that 5HT2a receptor activation shifts the network state towards criticality, which is consistent with multiple other findings related to the brain dynamics under the effects of psychedelic drugs (Girn et al., 2023).

We also report that the sensitivity to external perturbations covariates with the density of 5HT2a receptors. Since we normalized this value by the total number of nodes in each RSN, the explanation for this correlation should be found in the influence of 5HT2a in the organization of functional and structural connectivity. This serotonin receptor subtype is implicated in large-scale heterogeneities of the human cerebral cortex, constituting an important factor to distinguish between unimodal and the higher level integrative transmodal cortex (Luppi et al., 2023). Moreover, by bringing the global dynamics closer to dynamical criticality, 5HT2a receptor activation may facilitate the switching between inter-areal coupling that may underlying psychedelic-induced neural and cognitive flexibility (Doss et al., 2021), and also open a transient window where the increased functional diversity may exert an effect in the underlying structural connectivity via plasticity effects (Rocha et al., 2022), eventually consolidating the long-term effects associated with brief psychedelic episodes (Aday, Mitzkovitz, Bloesch, Davoli, & Davis, 2020). For high values of the external perturbation amplitude, the reactivity decoupled from the 5HT2a receptor density, likely indicating the saturation of the induced effects on whole-brain dynamics.

Beyond the current application, the temporal parametrization of whole-brain models may find other uses to test whether a certain temporal process underlies the recorded neuroimaging data, and to inform the potential mechanisms behind the empirical observations. The signal preprocessing steps applied to resting state fMRI data typically include high pass filters which are necessary to attenuate the effects of scanner drift and head movement (Cordes et al., 2001). Therefore, the fMRI time series may not directly reflect the dynamics of the phenomenon under study, unless the experiment is designed to maximize the signal-to-noise ratio, e.g. with tasks or stimulation structured in according to an adequate block design (Liu, Duffy, Bernal-Casas, Fang, & Lee, 2017). However, it may not be possible to control the onset and length of the temporal process under study, as in the current application to the study of a transient pharmacologically-induced event. This could also occur in the study of seizures (Chaudhary, Duncan, & Lemieux, 2013), sleep-related transients and graphoelements (e.g. spindles, K-complexes) (Duyn, 2012), spontaneous mentation or ongoing cognition (Brechet et al., 2019), and in other endogeneous phenomena with an interesting temporal structure but beyond experimental control. In these cases, the use of time-dependent whole-brain models may be useful to detect the fingerprints of the event in the FCD, by comparing different temporal parametrizations by fitting and contrasting their corresponding goodness of fit.

One important limitation of our approach is that the temporal parametrization a priori constraints the model and its capacity to detect the underlying temporal dynamics. By choosing a gamma function, our approach only allowed us to test whether the FCD dynamics under DMT could be better explained by this specific temporal evolution of the bifurcation parameter relative to the placebo condition. However, since we did not specify a prior the direction of the effect, this approach allowed us to test whether DMT could bring the dynamics closer to the global bifurcation and therefore towards a point of decreased stability. The choice of the gamma function can be justified by the prior literature on the time course of DMT-induced effects, as well as its effects on EEG activity and their correlation with the drug pharmacokinetics (Pallavicini et al., 2021; Strassman, 1996; Timmermann et al., 2023;

Timmermann et al., 2019). While more complex models could be implemented to adequately describe these dynamics (Eckernas et al., 2023), our choice has the merit of constituting a qualitative description of the transient effects of DMT without incurring in a proliferation of free parameters required for more neurobiological realism, which could difficult fitting the model to the empirical data. Moreover, the comparatively poor temporal resolution of fMRI may limit the potential gain of including a more nuanced description of pharmacodynamics.

In summary, our work shifted the focus from the reproduction of the steady-state effects of psychedelics towards disentangling the short-lasting effects of DMT. The future implementation of more realistic biophysical models could contribute to our understanding of how the interaction between drugs, neurotransmitters and receptors is capable of initiating a cascade of neural events which ultimately results in a global brain state with profound alterations in terms of consciousness and cognitive processing. The combination of these models with a more nuanced description of drug pharmacokinetics and pharmacodynamics could also contribute to explain the potential multiphasic effects of some psychedelic compounds, and to test potential mechanisms behind their long-lasting effects, which are a key aspect of their possible therapeutic use in patients with depression and other psychiatric disorders.

Materials and Methods

Study participants and experimental design

This is a re-analysis of a previously published EEG-fMRI dataset acquired from healthy participants under the acute effects of DMT (Timmermann et al., 2023). The original publication can be referenced for in-depth methodological details.

The study followed a single-blind, placebo-controlled design, with all participants providing written informed consent. The experimental protocol received approval from the National Research Ethics Committee London—Brent and the Health Research Authority, conducted in adherence to the Declaration of Helsinki (2000), International Committee on Harmonization Good Clinical Practices guidelines, and the National Health Service Research Governance Framework.

Volunteers engaged in two testing days at the Imperial College Clinical Imaging Facility, spaced two weeks apart. On each testing day, participants were subject to separate scanning sessions. In the initial session, they received intravenous administration of either placebo (10 mL sterile saline) or 20 mg DMT (fumarate form dissolved in 10 mL sterile saline). This was done in a counter-balanced order, with half receiving placebo and the rest receiving DMT. The first session comprised continuous resting-state scans lasting 28 minutes, with DMT/placebo administered at the end of the 8th minute, and scanning concluding 20 minutes after injection. Participants lay in the scanner with closed eyes aided by an eye mask, while fMRI data was recorded. In the second session, participants were cued to verbally rate the subjective intensity of drug effects every minute in real-time. Only fMRI data from the first scanning session was used for the present analysis.

A cohort of 20 participants completed all study visits, consisting of 7 females with a mean age of 33.5 years and a standard deviation of 7.9. For the present study only 15 of the subjects were used, the rest

being discarded due to strong head movement artifacts inside the scanner (see below for further information on the exclusion criterion).

fMRI acquisition and preprocessing

Images were acquired using a 3T MR scanner (Siemens Magnetom Verio syngo MR B17) with a 12-channel head coil for compatibility with EEG acquisition. Functional imaging was performed using a T2*-weighted BOLD-sensitive gradient echo planar imaging sequence [repetition time (TR) = 2000ms, echo time (TE) = 30 ms, acquisition time (TA) = 28.06 mins, flip angle (FA) = 80°, voxel size = 3.0 × 3.0 × 3.0mm3, 35 slices, interslice distance = 0 mm].

The preprocessing steps involved despiking, slice time correction, motion correction, brain extraction, rigid body registration to anatomical scans, nonlinear registration to 2mm MNI brain, and scrubbing (using an framewise displacement [FD] threshold of 0.4, with scrubbed volumes replaced by the mean of surrounding volumes) (Power, Barnes, Snyder, Schlaggar, & Petersen, 2012). Further steps included spatial smoothing (FWHM) of 6 mm, band-pass filtering between 0.01 and 0.08 Hz, linear and quadratic detrending, and regressing out nine nuisance regressors. These regressors, all band-pass filtered, consisted of six motion-related parameters (3 translations, 3 rotations) and three anatomically related parameters (ventricles, draining veins, local white matter). Finally, time series were extracted for each Automated Anatomical Labeling (AAL) (Tzourio-Mazoyer et al., 2002) template region by averaging the time series from all voxels within the corresponding region.

Out of 20 participants, five were excluded from group analyses due to excessive head movement during the 8-minute post-DMT period (>20% of scrubbed volumes with an framewise displacement threshold [FD] of 0.4).

Anatomical connectivity matrix

The anatomical connectivity matrix was obtained applying diffusion tensor imaging (DTI) on diffusion-weighted imaging (DWI) data obtained from 16 healthy right-handed participants (11 men and 5 women, mean age: 24.75 ± 2.54 years), recruited online at Aarhus University, Denmark. Participants with psychiatric or neurological disorders (or a history thereof) were excluded. For detailed MRI acquisition parameters, we refer readers to a previous publication. Anatomical connectivity networks were constructed in three steps. Firstly, whole-brain network regions were defined using the AAL atlas. Secondly, connections between nodes in the whole-brain network (edges) were estimated through probabilistic tractography applied to individual participant DTI data. Lastly, results were averaged across participants.

DTI preprocessing utilized the probtrackx tool from the FSL diffusion imaging toolbox (Fdt) (www.fsl.fmrib.ox.ac.uk/fsl/fslwiki/FDT) with default parameters. Subsequently, local probability distributions of fiber directions were estimated at each voxel. The connectivity probability from seed voxel i to another voxel j was defined as the proportion of fibers passing through voxel i that reached voxel j, with 5000 streamlines sampled per voxel. This process extended from the voxel to the region level, where in a region of interest consisting of n voxels, $5000 \times n$ fibers were sampled. The connectivity probability from region i to region j was calculated as the number of sampled fibers in region i that connected the two regions, divided by $5000 \times n$, where n represents the number of voxels in region i. The resulting anatomical connectivity matrices were then thresholded at 0.1% (equivalent to a minimum of five streamlines), yielding the anatomical connectivity matrices C_{ij} used in the model.

Whole-brain computational model

We simulated brain activity measured with fMRI at the whole-brain level by using a Stuard-Landau oscillator (i.e. Hopf normal form) for the local dynamics (see Fig. 1, "Local model"). This phenomenological model aims to directly simulate recorded brain signals. The emergent global dynamics are simulated by including mutual interactions between brain areas according to the anatomical connectivity matrix $\boldsymbol{C_{ij}}$ obtained from DTI (see Fig. 1, "Inter-areal coupling"). The full model consists of 90 coupled nodes representing the 90 cortical and subcortical brain areas from AAL parcellation, with the following temporal evolution for region $\boldsymbol{n}$:

$$\frac{dx_n}{dt} = (a(t) - {x_n}^2 - {y_n}^2)x_n - \omega y_n + G\sum_{p=1}^{90} C_{np}(x_p - \mathrm{x_n}) + \gamma\eta_\mathrm{n}(\mathrm{t})$$

$$\frac{\mathrm{dy_n}}{\mathrm{dt}} = (\mathrm{a(t)} - {\mathrm{x_n}}^2 - {\mathrm{y_n}}^2)\mathrm{x_n} + \omega_\mathrm{n}\mathrm{x_n} + \mathrm{G}\sum_{\mathrm{p=1}}^{90} \mathrm{C_{np}}(\mathrm{y_p} - \mathrm{y_n}) + \gamma\eta_\mathrm{n}(\mathrm{t}) \quad (1)$$

Here, η_n represents additive Gaussian noise with standard deviation γ (set to 0.05), $\mathrm{C_{np}}$ are the matrix elements of the anatomical connectivity matrix, G is a factor that scales the anatomical connectivity (fixed at G = 0.5, as determined previously in Ipina et al., 2020), ω_n is the peak frequency of node n in the 0.01-0.08 Hz band (determined using Fourier analysis applied to the empirical time series and averaged across participants), and variable $\mathrm{x_n}$ represents the empirical brain activity signal of node n, which was used to compute the simulated FC and FCD matrices.

The local dynamics present a supercritical bifurcation at a=0, so that if a>0 the system engages in a stable limit cycle (i.e. oscillations) with angular frequency ω_n, and when a<0 the local dynamics are attracted to a stable fixed point representing a low activity state dominated by noise. Close to the

bifurcation, the additive noise can induce a switching behavior between regimes, resulting oscillations with a complex envelope (Deco et al., 2017).

To model the short-lasting effects of DMT, we introduce a time-dependent bifurcation parameter $a(t)$ following a gamma function that represents a simplified description of drug pharmacokinetics (Salway & Wakefield, 2008):

$$a(t) = \lambda\left(\frac{te^{-t/\beta}}{N}\right) \tag{2}$$

where N is a constant that normalizes the term between brackets, λ is a scale parameter determining the amplitude of the peak, and β the parameter that controls the rate of decay of the function, and therefore is related to the latency of the peak (see Fig. 1, "Time dependency").

Model fitting to empirical data

To characterize the time-dependent structure of brain dynamics, we computed the FCD matrices (see Fig. 1, "Functional connectivity dynamics") (E. C. Hansen et al., 2015). For this purpose, each full-length signal of 28 min was split up into M = 82 sliding windows of 60 s each, with an overlap of 40 s between successive windows. For each sliding window centered at time t, the functional connectivity matrix FC(t) was computed. The FCD matrix is a $M \times M$ symmetric matrix whose t_1, t_2 entry is defined by the Pearson correlation coefficient between the upper triangular parts of the two matrices $FC(t_1)$ and $FC(t_2)$. These matrices were computed for each of the fifteen participants and simulations by exhaustively exploring the model parameters related to the temporal evolution of the bifurcation parameter, λ and β. To compare the FCD matrices taking into account their temporal

structure, we used the Frobenius distance between the elements of the empirical and simulated matrices.

Model fitting to baseline data

To set the model to the baseline conditions before the administration of the drug, we conducted a search for the best value of the bifurcation parameter by fitting the FCD submatrix of the first 22 temporal windows. This corresponds to the first 8 minutes previous to the injection of DMT. The fitting was done for both conditions (DMT and placebo) and as expected resulted in the same value of a = 0.07.

Fitting the temporal evolution of the bifurcation parameter

We fixed the value of the bifurcation parameter to the baseline value of a=0.07 for the first 8 minutes of the simulation and introduced the time dependency afterwards, given by the difference between the baseline value and the gamma function $\lambda\left(\frac{te^{-t/\beta}}{N}\right)$, with t=0 here indicating the time of the drug injection. Next, we performed an exhaustive exploration of the parameter space spanned by λ and β, searching for the optimal combination of parameters. For this purpose, we explored a grid given by λ = [0, 200] and β = [20, 900] in steps of 5 and 20 units, respectively. For each parameter combination, we computed the FCD 15 times (i.e. once per participant) randomly changing the initial conditions of the model. The resulting FCD matrices were averaged and compared with the empirical FCD using the Frobenius distance. This procedure was repeated 50 times for each pair of parameters.

Simulated perturbations

Next, we modeled an oscillatory perturbation and investigated the response of the whole-brain model fitted as explained in the previous section. The perturbation was given by an external additive periodic forcing term applied to node $\mathbf{n}$, $\mathbf{F_n} = \mathbf{F_{ext}}(\mathbf{cos}\,(\boldsymbol{\omega}_\mathbf{n}\mathbf{t}) + \mathbf{i}\,\mathbf{sin}\,(\boldsymbol{\omega}_\mathbf{n}\mathbf{t}))$, where the real part of the

perturbation is added to the equation for $\frac{\mathbf{dx_n}}{\mathbf{dt}}$ in Eq. 1 and the imaginary part to the equation for $\frac{\mathbf{dy_n}}{\mathbf{dt}}$. In the equation for $\mathbf{F_n}$, $\boldsymbol{\omega_n}$ is the natural frequency of the time series corresponding to node $\mathbf{n}$ (same as in Eq. 1).

To facilitate the interpretation of the results, we applied this perturbation to nodes located within six different resting state networks (RSN) identified using independent component analysis (ICA) by Beckmann et al. (2005). To account for the time variation of the reactivity, we sampled equally spaced values of $a(t)$, here noted a_p, with p indexing the time sample. Then, for every one of those values, we performed a simulation keeping a_p constant until the end of the simulation, i.e. for every simulation we set a=0.07 for the first 8 minutes and then the constant value, a_p until the end of the simulation. The perturbation was applied after the first 8 minutes corresponding to the baseline, varying the amplitude F_{ext} from 0 to 0.015 in 00125 steps. The maximum value of the range was chosen as it saturated the correlation between 5HT2a receptor density and local reactivity, as shown in Fig. 5. For each combination of RSN, F_{ext} and a_p we computed the resulting FCD and its distance to the empirical condition, and then assessed the impact of the perturbation as explained in the following section.

Measure of reactivity to perturbations

We interpret the whole-brain model reactivity as the sensitivity of brain activity to the external periodic stimulation. Following an analogy with the concept of susceptibility in statistical physics, we defined the reactivity as the following derivative:

$$\chi(t) = \frac{\partial M}{\partial F_{ext}}$$

(3)

where M denotes the Frobenius distance between the simulated and empirical FCD matrices. Therefore $\chi(t)$ quantifies how a certain RSN in a particular moment responds to an external perturbation in terms of its impact on the Frobenius metric. This magnitude was computed using a second order finite difference method. We evaluated $\chi(t)$ relative to its value at $t=0$. Furthermore, given that the number of nodes differs across the RSN, we computed the $\chi(t)$ normalized by the number of nodes of each RSN.

To determine the peak of $\chi(t)$ across the duration of the simulation, we used a bootstrapping procedure to obtain a distribution of peak values which allowed us to compute a confidence interval for the resulting average value. The bootstrap procedures were conducted by randomly drawing samples (with replacement) from the distribution of values, creating different $\chi(t)$ curves in each iteration and measuring its maximum value. The size of the sampled subset was equal to that of the original distribution. This procedure was repeated 200 times, generating a bootstrap distribution of the desired magnitude. When calculating the correlations between local 5HT2a receptor density and the maximum reactivity per RSN, the bootstrap was done 1000 times to generate the histograms.

Receptor density maps

The receptor density maps used were estimated using PET tracer studies obtained by Hansen and colleagues (J. Hansen, et al., 2021). All PET images were registered to the MNI-ICBM 152 nonlinear 2009 (version c, asymmetric) template and subsequently parcellated to the 90 region AAL atlas (Tzourio-Mazoyer et al., 2002). For more details on the acquisitions and limitations of the data set see the original publication (J. Hansen, et al., 2021).

Acknowledgments

ET is supported by PICT-2019–02294 (Agencia I+D+i, Argentina), ANID/FONDECYT Regular 1220995 (Chile) and by PIP 1122021010 0800CO (2022-2024) (CONICET, Argentina).

References

Aday, J. S., Mitzkovitz, C. M., Bloesch, E. K., Davoli, C. C., & Davis, A. K. (2020). Long-term effects of psychedelic drugs: A systematic review. *Neurosci Biobehav Rev, 113*, 179-189. doi:10.1016/j.neubiorev.2020.03.017

Beckmann, C. F., DeLuca, M., Devlin, J. T., & Smith, S. M. (2005). Investigations into resting-state connectivity using independent component analysis. *Philos Trans R Soc Lond B Biol Sci, 360*(1457), 1001-1013. doi:10.1098/rstb.2005.1634

Bedford, P., Hauke, D. J., Wang, Z., Roth, V., Nagy-Huber, M., Holze, F., . . . Diaconescu, A. O. (2023). The effect of lysergic acid diethylamide (LSD) on whole-brain functional and effective connectivity. *Neuropsychopharmacology, 48*(8), 1175-1183. doi:10.1038/s41386-023-01574-8

Brechet, L., Brunet, D., Birot, G., Gruetter, R., Michel, C. M., & Jorge, J. (2019). Capturing the spatiotemporal dynamics of self-generated, task-initiated thoughts with EEG and fMRI. *Neuroimage, 194*, 82-92. doi:10.1016/j.neuroimage.2019.03.029

Burt, J. B., Preller, K. H., Demirtas, M., Ji, J. L., Krystal, J. H., Vollenweider, F. X., . . . Murray, J. D. (2021). Transcriptomics-informed large-scale cortical model captures topography of pharmacological neuroimaging effects of LSD. *Elife, 10*. doi:10.7554/eLife.69320

Carhart-Harris, R. L., Leech, R., Hellyer, P. J., Shanahan, M., Feilding, A., Tagliazucchi, E., . . . Nutt, D. (2014). The entropic brain: a theory of conscious states informed by neuroimaging research with psychedelic drugs. *Front Hum Neurosci, 8*, 20. doi:10.3389/fnhum.2014.00020

Carhart-Harris, R. L., Muthukumaraswamy, S., Roseman, L., Kaelen, M., Droog, W., Murphy, K., . . . Nutt, D. J. (2016). Neural correlates of the LSD experience revealed by multimodal neuroimaging. *Proc Natl Acad Sci U S A, 113*(17), 4853-4858. doi:10.1073/pnas.1518377113

Carhart-Harris, R. L., Roseman, L., Haijen, E., Erritzoe, D., Watts, R., Branchi, I., & Kaelen, M. (2018). Psychedelics and the essential importance of context. *J Psychopharmacol, 32*(7), 725-731. doi:10.1177/0269881118754710

Chaudhary, U. J., Duncan, J. S., & Lemieux, L. (2013). Mapping hemodynamic correlates of seizures using fMRI: A review. *Hum Brain Mapp, 34*(2), 447-466. doi:10.1002/hbm.21448

Chialvo, D. R. (2010). Emergent complex neural dynamics. *Nature Physics, 6*, 744-750.

Cocchi, L., Gollo, L. L., Zalesky, A., & Breakspear, M. (2017). Criticality in the brain: A synthesis of neurobiology, models and cognition. *Prog Neurobiol, 158*, 132-152. doi:10.1016/j.pneurobio.2017.07.002

Cofre, R., Herzog, R., Mediano, P. A. M., Piccinini, J., Rosas, F. E., Sanz Perl, Y., & Tagliazucchi, E. (2020). Whole-Brain Models to Explore Altered States of Consciousness from the Bottom Up. *Brain Sci, 10*(9). doi:10.3390/brainsci10090626

Cordes, D., Haughton, V. M., Arfanakis, K., Carew, J. D., Turski, P. A., Moritz, C. H., . . . Meyerand, M. E. (2001). Frequencies contributing to functional connectivity in the cerebral cortex in "resting-state" data. *AJNR Am J Neuroradiol, 22*(7), 1326-1333. Retrieved from https://www.ncbi.nlm.nih.gov/pubmed/11498421

Deco, G., Cruzat, J., Cabral, J., Knudsen, G. M., Carhart-Harris, R. L., Whybrow, P. C., . . . Kringelbach, M. L. (2018). Whole-Brain Multimodal Neuroimaging Model Using Serotonin

Receptor Maps Explains Non-linear Functional Effects of LSD. *Curr Biol, 28*(19), 3065-3074 e3066. doi:10.1016/j.cub.2018.07.083

Deco, G., Kringelbach, M. L., Jirsa, V. K., & Ritter, P. (2017). The dynamics of resting fluctuations in the brain: metastability and its dynamical cortical core. *Sci Rep, 7*(1), 3095. doi:10.1038/s41598-017-03073-5

Demertzi, A., Tagliazucchi, E., Dehaene, S., Deco, G., Barttfeld, P., Raimondo, F., . . . Sitt, J. D. (2019). Human consciousness is supported by dynamic complex patterns of brain signal coordination. *Sci Adv, 5*(2), eaat7603. doi:10.1126/sciadv.aat7603

Dolder, P. C., Schmid, Y., Steuer, A. E., Kraemer, T., Rentsch, K. M., Hammann, F., & Liechti, M. E. (2017). Pharmacokinetics and Pharmacodynamics of Lysergic Acid Diethylamide in Healthy Subjects. *Clin Pharmacokinet, 56*(10), 1219-1230. doi:10.1007/s40262-017-0513-9

Doss, M. K., Povazan, M., Rosenberg, M. D., Sepeda, N. D., Davis, A. K., Finan, P. H., . . . Barrett, F. S. (2021). Psilocybin therapy increases cognitive and neural flexibility in patients with major depressive disorder. *Transl Psychiatry, 11*(1), 574. doi:10.1038/s41398-021-01706-y

Duyn, J. H. (2012). EEG-fMRI Methods for the Study of Brain Networks during Sleep. *Front Neurol, 3*, 100. doi:10.3389/fneur.2012.00100

Eckernas, E., Timmermann, C., Carhart-Harris, R., Roshammar, D., & Ashton, M. (2023). N,N-dimethyltryptamine affects electroencephalography response in a concentration-dependent manner-A pharmacokinetic/pharmacodynamic analysis. *CPT Pharmacometrics Syst Pharmacol, 12*(4), 474-486. doi:10.1002/psp4.12933

Girn, M., Rosas, F. E., Daws, R. E., Gallen, C. L., Gazzaley, A., & Carhart-Harris, R. L. (2023). A complex systems perspective on psychedelic brain action. *Trends Cogn Sci, 27*(5), 433-445. doi:10.1016/j.tics.2023.01.003

Gonzalez-Maeso, J., Weisstaub, N. V., Zhou, M., Chan, P., Ivic, L., Ang, R., . . . Gingrich, J. A. (2007). Hallucinogens recruit specific cortical 5-HT(2A) receptor-mediated signaling pathways to affect behavior. *Neuron, 53*(3), 439-452. doi:10.1016/j.neuron.2007.01.008

Hansen, E. C., Battaglia, D., Spiegler, A., Deco, G., & Jirsa, V. K. (2015). Functional connectivity dynamics: modeling the switching behavior of the resting state. *Neuroimage, 105*, 525-535. doi:10.1016/j.neuroimage.2014.11.001

Hansen, J., et al. (2021). Mapping neurotransmitter systems to the structural and functional organization of the human neocortex. *Biorxiv*.

Helfrich, R. F., Schneider, T. R., Rach, S., Trautmann-Lengsfeld, S. A., Engel, A. K., & Herrmann, C. S. (2014). Entrainment of brain oscillations by transcranial alternating current stimulation. *Curr Biol, 24*(3), 333-339. doi:10.1016/j.cub.2013.12.041

Herzog, R., Mediano, P. A. M., Rosas, F. E., Lodder, P., Carhart-Harris, R., Perl, Y. S., . . . Cofre, R. (2023). A whole-brain model of the neural entropy increase elicited by psychedelic drugs. *Sci Rep, 13*(1), 6244. doi:10.1038/s41598-023-32649-7

Holze, F., Becker, A. M., Kolaczynska, K. E., Duthaler, U., & Liechti, M. E. (2023). Pharmacokinetics and Pharmacodynamics of Oral Psilocybin Administration in Healthy Participants. *Clin Pharmacol Ther, 113*(4), 822-831. doi:10.1002/cpt.2821

Ipina, I. P., Kehoe, P. D., Kringelbach, M., Laufs, H., Ibanez, A., Deco, G., . . . Tagliazucchi, E. (2020). Modeling regional changes in dynamic stability during sleep and wakefulness. *Neuroimage, 215*, 116833. doi:10.1016/j.neuroimage.2020.116833

Jobst, B. M., Atasoy, S., Ponce-Alvarez, A., Sanjuan, A., Roseman, L., Kaelen, M., . . . Deco, G. (2021). Increased sensitivity to strong perturbations in a whole-brain model of LSD. *Neuroimage, 230*, 117809. doi:10.1016/j.neuroimage.2021.117809

Jobst, B. M., Hindriks, R., Laufs, H., Tagliazucchi, E., Hahn, G., Ponce-Alvarez, A., . . . Deco, G. (2017). Increased Stability and Breakdown of Brain Effective Connectivity During Slow-Wave Sleep: Mechanistic Insights from Whole-Brain Computational Modelling. *Sci Rep, 7*(1), 4634. doi:10.1038/s41598-017-04522-x

Kringelbach, M. L., Cruzat, J., Cabral, J., Knudsen, G. M., Carhart-Harris, R., Whybrow, P. C., . . . Deco, G. (2020). Dynamic coupling of whole-brain neuronal and neurotransmitter systems. *Proc Natl Acad Sci U S A, 117*(17), 9566-9576. doi:10.1073/pnas.1921475117

Kwan, A. C., Olson, D. E., Preller, K. H., & Roth, B. L. (2022). The neural basis of psychedelic action. *Nat Neurosci, 25*(11), 1407-1419. doi:10.1038/s41593-022-01177-4

Lebedev, A. V., Kaelen, M., Lovden, M., Nilsson, J., Feilding, A., Nutt, D. J., & Carhart-Harris, R. L. (2016). LSD-induced entropic brain activity predicts subsequent personality change. *Hum Brain Mapp, 37*(9), 3203-3213. doi:10.1002/hbm.23234

Liu, J., Duffy, B. A., Bernal-Casas, D., Fang, Z., & Lee, J. H. (2017). Comparison of fMRI analysis methods for heterogeneous BOLD responses in block design studies. *Neuroimage, 147*, 390-408. doi:10.1016/j.neuroimage.2016.12.045

Luppi, A. I., Carhart-Harris, R. L., Roseman, L., Pappas, I., Menon, D. K., & Stamatakis, E. A. (2021). LSD alters dynamic integration and segregation in the human brain. *Neuroimage, 227*, 117653. doi:10.1016/j.neuroimage.2020.117653

Luppi, A. I., Girn, M., Rosas, F. E., Timmermann, C., Roseman, L., Erritzoe, D., . . . Carhart-Harris, R. L. (2023). A role for the serotonin 2A receptor in the expansion and functioning of human transmodal cortex. *Brain*. doi:10.1093/brain/awad311

Marona-Lewicka, D., Thisted, R. A., & Nichols, D. E. (2005). Distinct temporal phases in the behavioral pharmacology of LSD: dopamine D2 receptor-mediated effects in the rat and implications for psychosis. *Psychopharmacology (Berl), 180*(3), 427-435. doi:10.1007/s00213-005-2183-9

Nichols, D. E. (2016). Psychedelics. *Pharmacol Rev, 68*(2), 264-355. doi:10.1124/pr.115.011478

Ort, A., Smallridge, J. W., Sarasso, S., Casarotto, S., von Rotz, R., Casanova, A., . . . Vollenweider, F. X. (2023). TMS-EEG and resting-state EEG applied to altered states of consciousness: oscillations, complexity, and phenomenology. *iScience, 26*(5), 106589. doi:10.1016/j.isci.2023.106589

Pallavicini, C., Cavanna, F., Zamberlan, F., de la Fuente, L. A., Ilksoy, Y., Perl, Y. S., . . . Tagliazucchi, E. (2021). Neural and subjective effects of inhaled N,N-dimethyltryptamine in natural settings. *J Psychopharmacol, 35*(4), 406-420. doi:10.1177/0269881120981384

Pedro A.M. Mediano, F. E. R., Christopher Timmermann, Leor Roseman, David J. Nutt, Amanda Feilding, Mendel Kaelen, Morten L. Kringelbach, Adam B. Barrett, Anil K. Seth, Suresh Muthukumaraswamy, Daniel Bor, View Robin L. Carhart-Harris. (2024). Effects of external stimulation on psychedelic state neurodynamics. *ACS Chem Neurosci*.

Piccinini, J., Ipinna, I. P., Laufs, H., Kringelbach, M., Deco, G., Sanz Perl, Y., & Tagliazucchi, E. (2021). Noise-driven multistability vs deterministic chaos in phenomenological semi-empirical models of whole-brain activity. *Chaos, 31*(2), 023127. doi:10.1063/5.0025543

Power, J. D., Barnes, K. A., Snyder, A. Z., Schlaggar, B. L., & Petersen, S. E. (2012). Spurious but systematic correlations in functional connectivity MRI networks arise from subject motion. *Neuroimage, 59*(3), 2142-2154. doi:10.1016/j.neuroimage.2011.10.018

Preller, K. H., Burt, J. B., Ji, J. L., Schleifer, C. H., Adkinson, B. D., Stampfli, P., . . . Anticevic, A. (2018). Changes in global and thalamic brain connectivity in LSD-induced altered states of consciousness are attributable to the 5-HT2A receptor. *Elife, 7*. doi:10.7554/eLife.35082

Rocha, R. P., Kocillari, L., Suweis, S., De Filippo De Grazia, M., de Schotten, M. T., Zorzi, M., & Corbetta, M. (2022). Recovery of neural dynamics criticality in personalized whole-brain models of stroke. *Nat Commun, 13*(1), 3683. doi:10.1038/s41467-022-30892-6

Salway, R., & Wakefield, J. (2008). Gamma generalized linear models for pharmacokinetic data. *Biometrics, 64*(2), 620-626. doi:10.1111/j.1541-0420.2007.00897.x

Schartner, M. M., Carhart-Harris, R. L., Barrett, A. B., Seth, A. K., & Muthukumaraswamy, S. D. (2017). Increased spontaneous MEG signal diversity for psychoactive doses of ketamine, LSD and psilocybin. *Sci Rep, 7*, 46421. doi:10.1038/srep46421

Singleton, S. P., Luppi, A. I., Carhart-Harris, R. L., Cruzat, J., Roseman, L., Nutt, D. J., . . . Kuceyeski, A. (2022). Receptor-informed network control theory links LSD and psilocybin to a flattening of the brain's control energy landscape. *Nat Commun, 13*(1), 5812. doi:10.1038/s41467-022-33578-1

Solovey, G., Alonso, L. M., Yanagawa, T., Fujii, N., Magnasco, M. O., Cecchi, G. A., & Proekt, A. (2015). Loss of Consciousness Is Associated with Stabilization of Cortical Activity. *J Neurosci, 35*(30), 10866-10877. doi:10.1523/JNEUROSCI.4895-14.2015

Strassman, R. J. (1996). Human psychopharmacology of N,N-dimethyltryptamine. *Behav Brain Res, 73*(1-2), 121-124. doi:10.1016/0166-4328(96)00081-2

Tagliazucchi, E., Carhart-Harris, R., Leech, R., Nutt, D., & Chialvo, D. R. (2014). Enhanced repertoire of brain dynamical states during the psychedelic experience. *Hum Brain Mapp, 35*(11), 5442-5456. doi:10.1002/hbm.22562

Tagliazucchi, E., Roseman, L., Kaelen, M., Orban, C., Muthukumaraswamy, S. D., Murphy, K., . . . Carhart-Harris, R. (2016). Increased Global Functional Connectivity Correlates with LSD-Induced Ego Dissolution. *Curr Biol, 26*(8), 1043-1050. doi:10.1016/j.cub.2016.02.010

Tian, Y., Tan, Z., Hou, H., Li, G., Cheng, A., Qiu, Y., ... & Sun, P. (2022). Theoretical foundations of studying criticality in the brain. *Network Neuroscience, 6(4)*, 1148-1185.

Timmermann, C., Roseman, L., Haridas, S., Rosas, F. E., Luan, L., Kettner, H., . . . Carhart-Harris, R. L. (2023). Human brain effects of DMT assessed via EEG-fMRI. *Proc Natl Acad Sci U S A, 120*(13), e2218949120. doi:10.1073/pnas.2218949120

Timmermann, C., Roseman, L., Schartner, M., Milliere, R., Williams, L. T. J., Erritzoe, D., . . . Carhart-Harris, R. L. (2019). Neural correlates of the DMT experience assessed with multivariate EEG. *Sci Rep, 9*(1), 16324. doi:10.1038/s41598-019-51974-4

Tzourio-Mazoyer, N., Landeau, B., Papathanassiou, D., Crivello, F., Etard, O., Delcroix, N., . . . Joliot, M. (2002). Automated anatomical labeling of activations in SPM using a macroscopic anatomical parcellation of the MNI MRI single-subject brain. *Neuroimage, 15*(1), 273-289. doi:10.1006/nimg.2001.0978

Viol, A., Palhano-Fontes, F., Onias, H., de Araujo, D. B., & Viswanathan, G. M. (2017). Shannon entropy of brain functional complex networks under the influence of the psychedelic Ayahuasca. *Sci Rep, 7*(1), 7388. doi:10.1038/s41598-017-06854-0

Wallach, J., Cao, A. B., Calkins, M. M., Heim, A. J., Lanham, J. K., Bonniwell, E. M., . . . McCorvy, J. D. (2023). Identification of 5-HT(2A) receptor signaling pathways associated with psychedelic potential. *Nat Commun, 14*(1), 8221. doi:10.1038/s41467-023-44016-1

Zamberlan, F., Sanz, C., Martinez Vivot, R., Pallavicini, C., Erowid, F., Erowid, E., & Tagliazucchi, E. (2018). The Varieties of the Psychedelic Experience: A Preliminary Study of the Association Between the Reported Subjective Effects and the Binding Affinity Profiles of Substituted Phenethylamines and Tryptamines. *Front Integr Neurosci, 12*, 54. doi:10.3389/fnint.2018.00054